Equilibrium crystal shapes for lattice models with nearest- and next-nearest-neighbor interactions

Craig Rottman* and Michael Wortis
Department of Physics and Materials Research Laboratory, University of Illinois at Urbana—Champaign, 1110 W. Green Street, Urbana, Illinois 61801
(Received 29 August 1983)

Equilibrium crystal shapes for a three-dimensional ferromagnetic Ising model with both nearest-neighbor (J_1) and next-nearest-neighbor ($J_2=RJ_1$) interactions are studied at nonzero temperatures. Phase diagrams and crystal shapes are first calculated via mean-field theory. Subsequently, fluctuation corrections are taken into account in a qualitative manner, incorporating known results and exploiting interconnections with other ($d=2$) models, including both roughening and commensurate-incommensurate phase transitions. In the resulting picture, crystal facets appear only below appropriate roughening temperatures. Phase boundaries correspond directly to edges bounding crystal facets and may be either first order (slope discontinuity, sharp edges) or second order (no slope discontinuity, smooth edges). For $R \geq 0$, only smooth edges occur, and phase transitions are of the Gruber-Mullins—Pokrovsky-Talapov type. For $R<0$ additional, first-order phase transitions take place at sufficiently low temperatures.

I. INTRODUCTION

At ordinary first-order two-phase bulk coexistence a large inclusion of one phase may remain in stable equilibrium with a background of the other. The average shape of the inclusion is then determined by strictly thermodynamic considerations,[1-3] which involve minimizing the free energy of creating the necessary interfacial boundaries. When both the coexisting phases are isotropic, the shape of the inclusion is spherical. When one or both are crystalline or otherwise anisotropic, interfaces of some orientations are preferred over those of the other orientations, and the "equilibrium crystal shape" (ECS) of the inclusion is nonspherical and may be more or less complex. Two limiting cases are completely faceted shapes (polyhedra), consisting entirely of strictly planar faces (facets) joined at sharp edges, and completely rounded shapes, which are smoothly curved everywhere and lack both facets and edges. Between these two extremes are shapes containing both rounded and faceted regions[4] joined at edges which may be either "sharp" (slope discontinuity) or "smooth" (no slope discontinuity). Both sharp and smooth edges have been seen in experiments.[3,5,6] The equilibrium shape of a typical crystal evolves with temperature T from completely faceted at $T=0$ to partially or completely rounded at sufficiently high temperature. It is the purpose of this paper to study this evolution on the basis of statistical mechanics and in the context of a simple three-dimensional ($d=3$) ferromagnetic Ising model, equivalent to an attractive lattice gas. Two phases ("up" and "down") coexist in this model for all $T<T_c$ (the bulk critical temperature). Anisotropy is provided by the lattice and disappears progressively as $T \to T_c^-$. Despite its simplicity, the model exhibits a thermal evolution which is qualitatively similar to that of real crystals.[5,6] In particular, it provides insight into the important effects of further-neighbor interactions, and it leads to a plausible identification of the universality classes of the interfacial phase transitions which occur in nature.

Several models have been studied in the past to try to understand ECS features from statistical mechanical considerations. In $d=2$, exact results are available for certain nearest-neighbor lattice models.[7] The ECS is smoothly curved everywhere for $T>0$. Hereinafter we will concern ourselves with $d=3$ crystal shapes. At $T=0$, crystal shapes are easy to calculate and turn out to be completely faceted for lattice (Ising) models with interactions of finite range.[8] For $T>0$, no exact results are available and it has been traditional, since the celebrated work of Burton, Cabrera, and Frank,[9] to explore models in which the interface is microscopically sharp and no bulk fluctuations are allowed. Such $d=2$ solid-on-solid (SOS) models can be built to incorporate the most important low-temperature interfacial excitations, steps[10,11] (necessary to describe macroscopic tilting away from symmetry directions), and thermal fluctuations[12,13] (necessary to describe roughening[14]). Special models of this type can be solved exactly.[10-13] Most recently, such a model has been used[13] to describe in detail the mechanism by which a facet shrinks and finally disappears as the temperature is raised through the appropriate roughening temperature T_R. These models are, of course, fully appropriate only at low temperatures (where bulk excitations are rare) and for low tilt angles (where the SOS restriction preventing overhangs is reasonable). Furthermore, they are exactly soluble only with nearest-neighbor interactions.

An alternative approach, which we shall follow here, is to work directly with the $d=3$ lattice model, which allows bulk excitations and overhangs and is, therefore, appropriate over the full range of temperatures and tilt angles. Exact solution is not possible; however, we extend some early work by Lacmann[15] to obtain a complete picture of the in-

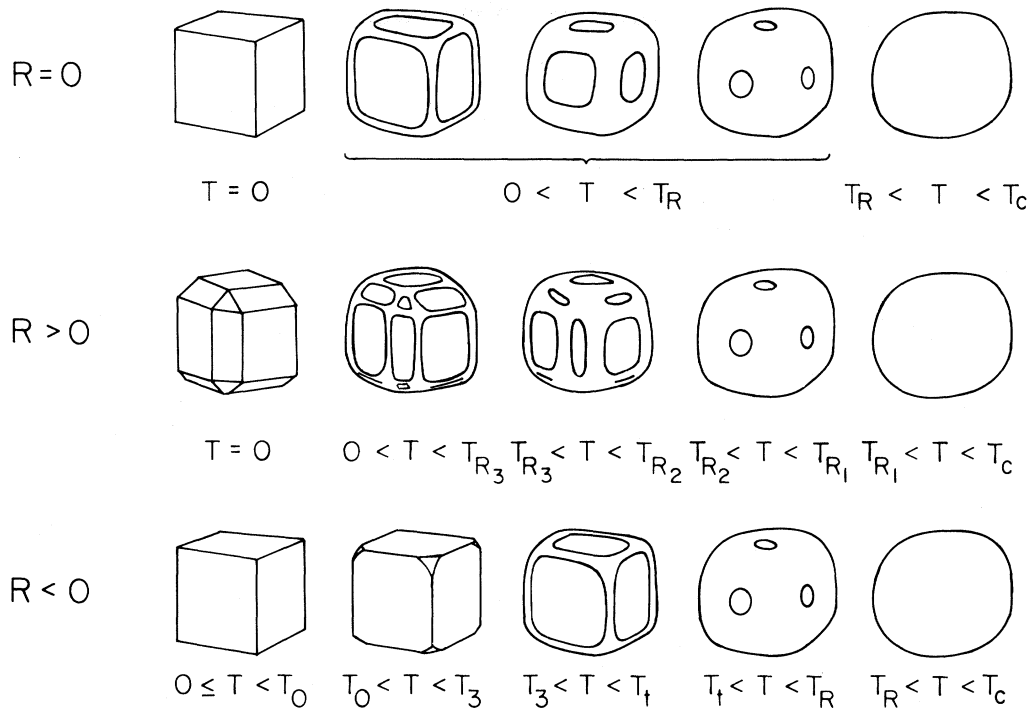

FIG. 1. Equilibrium crystal shapes for a lattice-gas model with both NN (J_1) and NNN ($J_2=RJ_1$) interactions. For $R=0$, the crystal shape evolves from cubical ($T=0$) to spherical ($T=T_c$). Below the {100} roughening temperature T_R, rounded regions separate {100} facets and edges are smooth everywhere. Above T_R, the crystal shape is completely rounded. $R>0$ is similar to $R=0$ except that additional {110} and {111} facets are found at low temperatures. For $R<0$, the cubic shape is now stable for $0\leq T\leq T_0$. Sharp edges remain above T_0, and the last piece of sharp edge disappears at T_t.

terfacial phase diagrams *within the mean-field approximation.* This approach leads to calculations which are simple enough to permit study of the effects of further-neighbor interactions. Unfortunately, the mean-field approximation misses entirely certain fluctuation-dominated phenomena such as roughening.[16] This deficiency has been studied in some detail in other closely analogous situations.[17–24] By drawing on these parallels to supplement mean-field information, it is possible to construct qualitative interfacial phase diagrams and corresponding crystal shapes for our model which, although certainly not rigorous, are probably correct.

The results at which we arrive are summarized in Fig. 1. The model has only nearest-neighbor interactions ($J_1>0$) and next-nearest-neighbor interactions ($J_2=RJ_1$). When $R=0$ (nearest neighbor only) the ECS is cubical at $T=0$. At low but nonzero T, {100} facets remain but are now separated by rounded regions. Edges are always smooth. Facets shrink with increasing T and finally disappear at the {100} roughening temperature T_R, above which the ECS is completely rounded. $R>0$ differs from $R=0$ in that, at sufficiently low T, {111} and {110} facets are found in addition to {100} facets. As T is increased, each set of facets disappears at its own roughening temperature in the order indicated. For $R<0$, on the other hand, the ECS remains cubical from $T=0$ up to a nonzero temperature T_0. Rounded surfaces first appear at the cube corners. Smooth and sharp edges are both encountered, as we shall discuss in more detail below.

The outline of this paper is as follows. The remainder of this section will serve as a brief introduction to the idea of interfacial phase diagrams. Section II A describes the model and defines the interfacial free energy per unit area $f_i(T,\hat{m})$, where $\hat{m}$ specifies the interface orientation relative to the crystal axes. The Wulff construction[1,2,25,26] reviewed in Sec. II B supplies the connection between $f_i(T,\hat{m})$ and the ECS $r(T,\hat{h})$, where r measures the radius in direction $\hat{h}$ from the center of the crystal. Section II C presents the exact analysis at $T=0$. Mean-field results are displayed in Sec. III. Calculational details are relegated to an Appendix. In Sec. IV we propose and defend what we believe the exact interfacial phase diagrams should look like.

A thermodynamic phase diagram is by definition a plot of the loci of singularities of a certain intensive free energy. We shall use two types of interfacial phase diagrams, that based on the interfacial free energy $f_i(T,\hat{m})$ and that based on the crystal shape itself $r(T,\hat{h})$. The fact that $r(T,\hat{h})$ may be regarded as a free energy[3] may at first seem surprising. This connection was first established by Andreev,[27] who showed that the pairs $\hat{m},f$ and $\hat{h},r$ are conjugate under Legendre transformation. The singularities at fixed T of $r(T,\hat{h})$ occur at the crystal edges discussed above: Sharp edges (slope discontinuity) correspond to first-order phase transitions and smooth edges (no slope discontinuity) to second-order phase transitions. Although conjugate, the $\hat{m}$ and $\hat{h}$ variables have somewhat different character. $\hat{h}$ is a "field" variable in that r is well defined for all $\hat{h}$. $\hat{m}$ by contrast is a "density" variable in

that it may happen that certain $\hat{m}$ values are not attainable at equilibrium. This leads to forbidden regions in the $(T,\hat{m})$ phase diagram and takes place (for example, at $R<0$ in our model) when the presence of sharp edges or points eliminates certain orientations $\hat{m}$ from the surface of the ECS. Interfacial orientations not present on the ECS are unstable to the formation of hill-and-valley structures[1,2] in a dynamic process called "thermal faceting,"[28] which represents interfacial phase separation.[29] Although the $(T,\hat{m})$ and $(T,\hat{h})$ phase diagrams contain the same information, we shall find the $(T,\hat{h})$ representation particularly convenient: It is simply related to the thermal evolution of the ECS (Fig. 1) and, therefore, easily visualizable. Furthermore, it provides the more direct link with the analog systems[17–24] which we use (Sec. IV) to supplement our mean-field calculations.

II. EXACT RESULTS

A. The model

We chose to study the Ising model on a simple cubic lattice of N sites ($N=L\times L\times L$) with both nearest-neighbor (NN) and next-nearest-neighbor (NNN) interactions,

$$\mathscr{H}=-J_1\sum_{\substack{\langle ij\rangle\\ \text{NN}}}\sigma_i\sigma_j-J_2\sum_{\substack{\langle ij\rangle\\ \text{NNN}}}\sigma_i\sigma_j,\quad \sigma_i=\pm 1\ . \tag{1}$$

For simplicity we restrict our attention to $J_1>0$ and small $|R|$, where $R=J_2/J_1$, so that the bulk phase is ferromagnetic. The equivalent lattice-gas model[30] comes about by identifying a local particle-density variable $n_i=(1+\sigma_i)/2=0,1$. The absence of any (odd) magnetic field term in the Hamiltonian (1) places the system for $0\le T\le T_c$ on a first-order phase boundary between "up" ($\langle\sigma_i\rangle>0$, lattice-gas "solid") and "down" ($\langle\sigma_i\rangle<0$, lattice-gas "fluid") bulk phases.

To define the interfacial free energy $f_i(T,\hat{m})$ it is necessary to control boundary conditions so as to be able to produce an interface of specified orientation $\hat{m}$. For $\{100\}$ orientations this is easily achieved[31,32] by applying periodic boundary conditions, and then changing the sign of the couplings J_1 and J_2 which cross (any) one particular (100) plane. We denote by $\mathscr{H}'$ the Hamiltonian with these reversed interactions. The interfacial free energy per unit area associated with the interfaces thus forced is identified as

$$f_i(T,\hat{m})=-k_BT\lim_{L\to\infty}\frac{1}{L^2}(\ln \mathrm{Tr}\, e^{-\beta\mathscr{H}'}-\ln \mathrm{Tr}\, e^{-\beta\mathscr{H}})\ , \tag{2}$$

in which the (bulk) contribution, not associated with the interface, has been subtracted out. Note that f_i vanishes for $T\ge T_c$. Generalization of this technique to off-axis orientations involves using appropriately twisted periodic boundary conditions and putting in the corresponding geometrical correction to the interfacial area (which is no longer L^2). Further details are given in the Appendix. In practice we have performed most (but not all[33]) of our calculations for interfaces parallel to the $\hat{z}$ axis, $\hat{m}=(\cos\theta,\sin\theta,0)$. Because of the cubic symmetry,

$$f_i(\theta)=f_i(\theta+\pi/2)=f_i(\pi/2-\theta)\ , \tag{3}$$

so it is only necessary to calculate for angles $0\le\theta\le\pi/4$. To make the symmetry more visible, we shall take in phase diagrams $0\le\theta\le\pi/2$, $0\le T\le T_c$ for each (fixed) value of R.

B. The Wulff construction

Once $f_i(T,\hat{m})$ is known, the ECS follows from the Wulff construction.[1–3,25] In particular, $f_i(T,\theta)$ generates an equatorial section ($z=0$) through the full ECS $r(T,\hat{h})$, covering a range of orientations $\hat{h}=(\cos\phi,\sin\phi,0)$ with $0\le\phi<2\pi$. The curved regions of $r(\phi)$ follow from $f_i(\theta)$ via[26]

$$\begin{aligned} x&=(\cos\theta)f_i-(\sin\theta)\frac{df_i}{d\theta},\quad r=r_0(x^2+y^2)^{1/2}\ ,\\ y&=(\sin\theta)f_i+(\cos\theta)\frac{df_i}{d\theta},\quad \tan\phi=y/x\ . \end{aligned} \tag{4}$$

Facets in $r(\phi)$ arise from cusps in $f_i(\theta)$ and have corresponding orientations. $r(\phi)$ has cubic symmetry analogous to Eq. (3).

C. $T=0$ behavior

At $T=0$ the interfacial free energy $f_i(T=0,\hat{m})$ is just the minimum energy per unit area required to produce an interface of macroscopic orientation $\hat{m}$. Evaluation can be achieved by direct counting of the number of broken bonds induced.[1,8] For $\hat{m}=(\cos\theta,\sin\theta,0)$ results are[34] (where $c\equiv\cos\theta$, $s\equiv\sin\theta$)

$$f_i(T=0,\theta)=\begin{cases}2J_1(|c|+|s|)+2J_2(2|c|+2|s|+|c+s|+|c-s|), & R\ge 0\\ (2J_1+8J_2)(|c|+|s|), & R\le 0\end{cases} \tag{5}$$

and the equilibrium crystal shapes are as given in Fig. 1. For $R\le 0$ ($J_2\le 0$) the singularities of $f_i(T=0,\hat{m})$ are cusps in the symmetry directions $\hat{m}=\{100\}$ and the ECS is cubical [with singularities in $r(T=0,\phi)$ at the cube edges $\phi=\pm\pi/4,\pm 3\pi/4$]. For $R>0$ ($J_2>0$) additional cusps appear for directions $\hat{m}=\{110\}$ and $\{111\}$, and the corresponding facets show up on the ECS. In particular, $r(T=0,\phi)$ is now singular at angles ϕ_c where $\{100\}$ and $\{110\}$ facets meet,

$$|\tan\phi_c|=\frac{1+2R}{1+4R}\quad\text{and}\quad|\cot\phi_c|=\frac{1+2R}{1+4R}\ . \tag{6}$$

A special degeneracy attaches to the point $R=T=0$: Because $J_2=0$, the energy of a microscopic interface con-

figuration of overall orientation $\hat{m}$ depends only on the total microscopic interfacial area (and not on the number of edges, corners, etc.). The minimum-energy state (which is just the minimum-area state) is, therefore, highly degenerate, unless $\hat{m}$ is a $\{100\}$ direction. One of this set of degenerate configurations uses only macroscopic $\{100\}$ planes. As a consequence, the Wulff construction is marginal: The $\{100\}$ directions of $\hat{m}$ contribute the entire area of the ECS, while all other orientations have Wulff planes which pass only through edges or corners of the ECS. This degeneracy and its associated marginality makes behavior near $R=T=0$ especially sensitive to small changes in the interparticle interactions, etc., and accounts for important qualitative features of the phase diagrams which we shall map out in Secs. III and IV. At $R=0$, the high degeneracy is associated with the fact that the phase boundaries near $\phi=\pm\pi/4,\pm 3\pi/4$ become second order for $T>0$. At $T=0$, on the other hand, $R=0$ is the borderline between two rather different behaviors. For $R<0$, edges and corners are energetically disfavored, and the degeneracy noted above is broken in favor of the maximally planar microscopic configurations. This has the effect of eliminating entirely the orientations $\hat{m}\neq\{100\}$ from the ECS, thus stabilizing the sharply faceted, cubical shape up to a nonzero temperature (orientations $\hat{m}\neq\{100\}$ are regions of first-order coexistence of the phase diagram at and near $T=0$). For $R>0$, edges and corners are favored. For interactions which do not extend beyond NNN's, this lifts the degeneracy in the $\{110\}$ and $\{111\}$ directions and leads to the appearance of the corresponding facets on the ECS. The degeneracy is reduced but not eliminated for other directions, and phase boundaries become second order (with rounding of sharp $T=0$ edges) for $T>0$. Additional further-neighbor interactions would lead to new $T=0$ facets.

III. MEAN-FIELD RESULTS

Mean-field calculation of the interfacial free energy per unit area $f_i(T,\hat{m})$ is described in the Appendix. We have concentrated mainly on the equatorial plane $\hat{m}=(\cos\theta,\sin\theta,0)$, with supplemental work at $\hat{m}=\{111\}$. Calculation is greatly simplified by choosing orientations $\hat{m}$ which give periodic structure in the plane of the interface. Thus we take

$$\tan\phi=p/q\ , \tag{7}$$

where p and q are positive integers and relatively prime, $0\leq p\leq q\leq 10$. This allows 33 distinct values of θ in the range 0–$\pi/4$, for which we have calculated $f_i(T,\theta)$ for

$$0\leq T\leq T_c=(6J_1+12J_2)/k_B\ .$$

Using these data, we then carried through the Wulff construction. Because the set of angles θ is discrete, the result is a completely faceted, polygonal ECS in which all edges are sharp (first order). The angular positions ϕ of those edges are plotted in Fig. 2 for $R=0$. Notice that for $T>0$ facets of all possible orientations appear. To generate the full mean-field (T,ϕ) phase diagram it is now necessary to imagine taking the angular grid (θ) finer and finer to approach the continuum limit. Based on our calculations

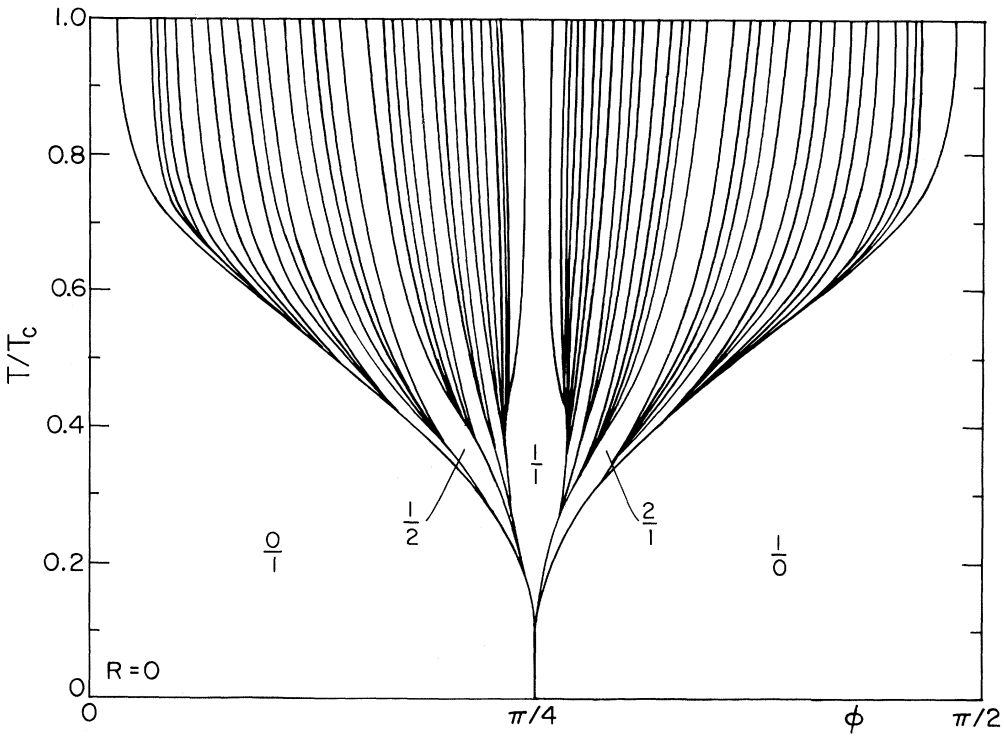

FIG. 2. Angular positions ϕ of the edges between facets calculated within mean-field theory for $R=0$. The mean-field free energy $f_i(T,\theta)$ is calculated for a finite number of orientations θ, resulting in a completely faceted crystal shape. The true mean-field phase diagram is found by including all values of θ (continuum limit).

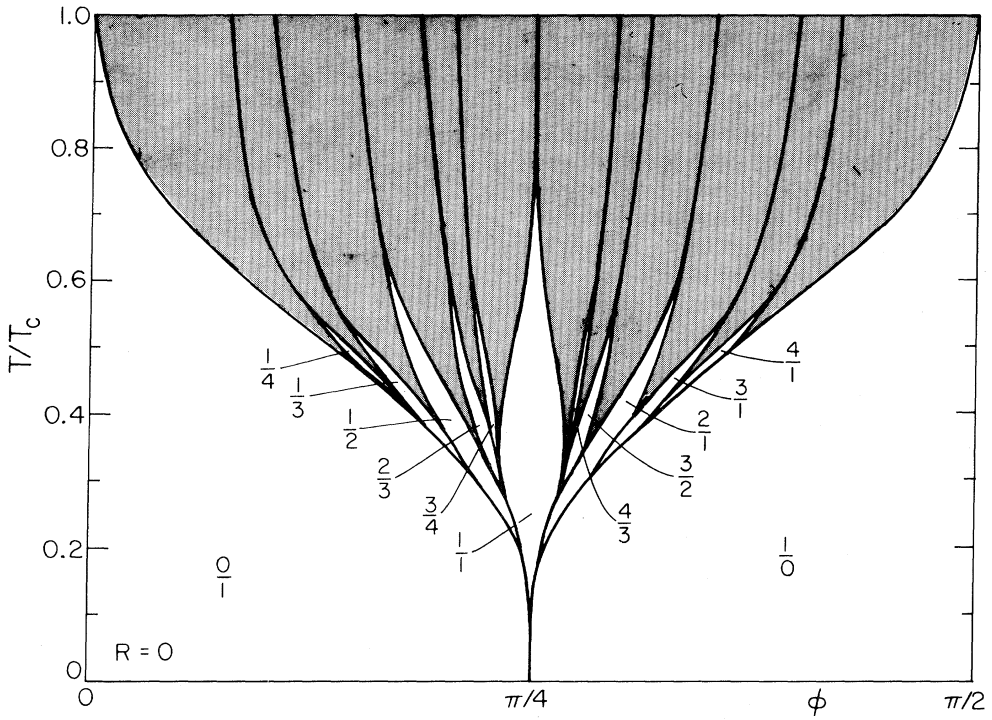

FIG. 3. Mean-field (ϕ, T) phase diagram for $R=0$, obtained by eyeball extrapolation of Fig. 2 to the continuum limit. Lines running between $T=T_c$ and $T=0$ give the angular position ϕ of edges of facets. Only low-order facets are included. Values of $\tan\theta=p/q$ are labeled (θ characterizes facet orientation). Shaded regions contain higher-order facets. Numerical evidence suggests that all facets occur for $T>0$.

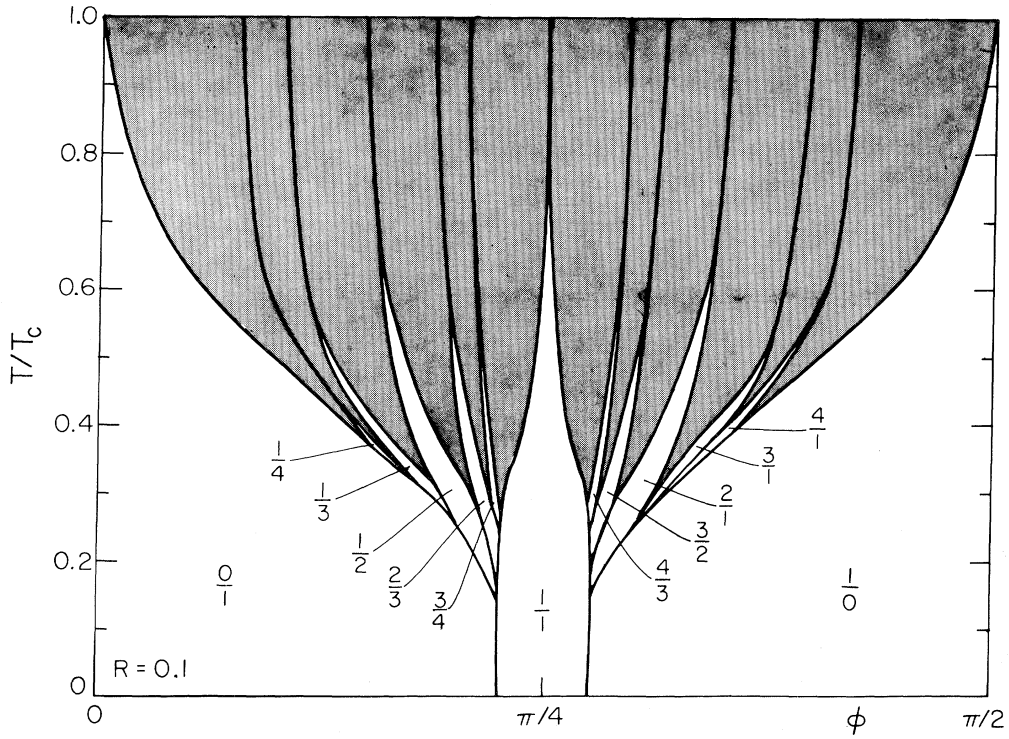

FIG. 4. Mean-field (ϕ, T) phase diagram for $R=0.1$. Note that $\{110\}$ facets are now present at $T=0$. Numerical evidence again suggests that all facets occur for $T>0$.

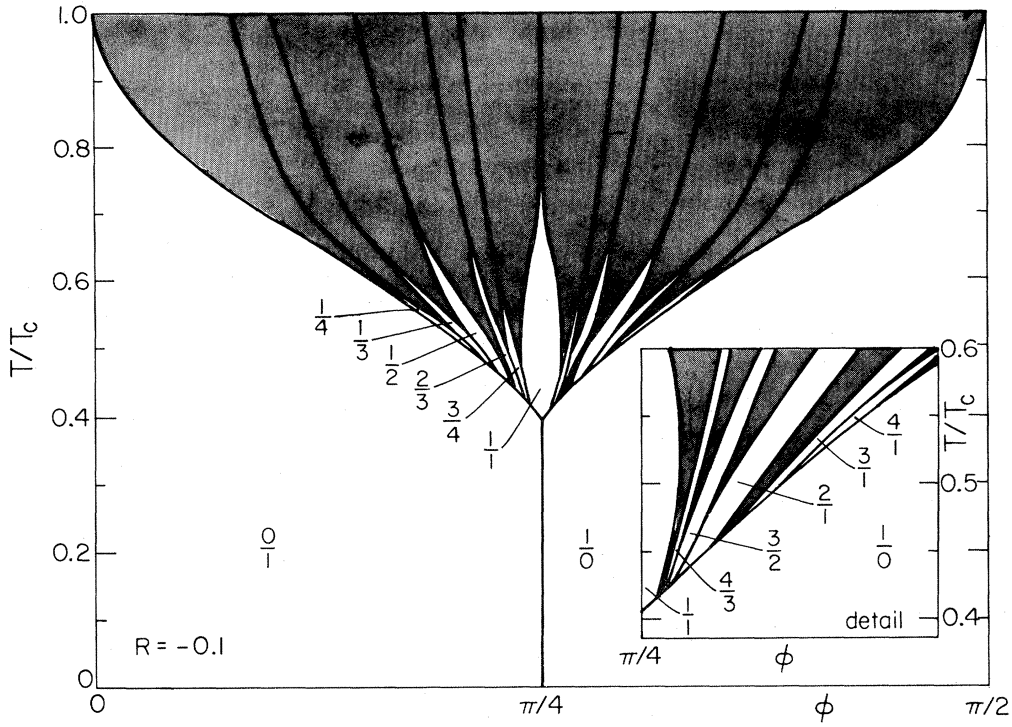

FIG. 5. Mean-field (ϕ,T) phase diagram for $R=-0.1$. Facets of all orientations are now present only for $T/T_c \gtrsim 0.55$. At low temperatures ($T/T_c \lesssim 0.28$) the ECS is strictly cubic. Rounded surfaces first appear at the cube corners and only reach the equatorial plane (shown here) at $T/T_c \simeq 0.4$. For $0.28 \lesssim T/T_c \lesssim 0.55$, facets of some orientations are still missing, so that certain edges remain sharp.

with $q \leq 10$, it appears entirely plausible that, for each additional θ included, an additional line shows up in Fig. 2, running between $T=T_c$ and $T=0$. It does *not* follow, however, that these lines (edges) become dense everywhere in Fig. 2, converting the ECS into a smoothly rounded figure. On the contrary, there is already good evidence in Fig. 2 that certain regions of ϕ remain edge free in the continuum limit. These edge-free regions correspond to planar facets of the ECS. To find their outlines rigorously would require studying the large-q limit, which is beyond our present program. Nevertheless, the low-order facets ($q=1,2,3,4$) can be picked out with good accuracy from Fig. 2. The result, shown in Fig. 3, takes advantage of the fact that[35] f_i becomes independent of θ as $T \to T_c^-$, so the angular width of all facets goes to zero in this limit. At $T=0$, only $\{100\}$ facets are present, in agreement with Sec. II C. For $T>0$ low-index (small-q) facets are largest, especially at low temperatures; however, the numerical evidence is consistent with the propositions that rational facets are dense in ϕ and that for $T>0$ all rational facets would appear at sufficiently high resolution.[36] If so, the situation is analogous to what happens in mean-field treatments of the anisotropic NNN Ising (ANNNI) model.[22,23] The picture[36] which emerges then from mean-field theory at $R=0$ is an ECS which is cubical at $T=0$, but, at $T>0$, develops facets at all rational orientations, evolving continuously to a uniformly rounded shape at $T=T_c$. Since all orientations occur, edges are smooth (second order). The corresponding $(T,\hat{m})$ phase diagram is completely dense with phase boundaries, since for $0<T<T_c$, the Wulff plot must have cusps at all rational orientations.[37] We shall consider in Sec. IV the modifications of these mean-field phase diagrams by fluctuations. For the moment, we consider the effect of nonzero NNN interactions J_2.

Figures 4 and 5 are the analogs of Fig. 3 for $R=0.1$ ($R>0$) and $R=-0.1$ ($R<0$), respectively. For positive R, the $\{100\}$, $\{110\}$, and $\{111\}$ facets (only) are present at $T=0$ (Sec. II C). Numerical evidence again suggests[36] that all facets occur for $T>0$, with gradual evolution towards a smoothly rounded shape as $T \to T_c^-$. For negative R, the evolution is quite different, and the stabilization of the $\{100\}$ facets (Sec. II C) shows up clearly. The lines (edges) in the representation of Fig. 2 start at $T=T_c$ but now terminate at $T>0$ against the (100) and (010) facets. The cubical ECS is maintained well above $T=0$. Further faceting does not occur for $R=-0.1$ until $T/T_c \simeq 0.28$, when the $\{111\}$ facets first appear at the cube corners. The equatorial plane (shown in Fig. 5) remains square until $T/T_c \simeq 0.4$, and it is only for $T/T_c \gtrsim 0.55$ that all rational facets occur on the ECS. For $0.28 \lesssim T/T_c \lesssim 0.55$, facets of some orientations are still missing, and certain edges of the $\{100\}$ facets are sharp (first order).

IV. BEYOND MEAN-FIELD THEORY

The mean-field results of Sec. III neglect fluctuation effects and are, therefore, expected to be quantitatively and even qualitatively wrong when such effects play an important role. Fluctuation effects are known in other contexts

to be particularly important near second-order phase transitions and generally in two dimensions (the reader is reminded that the interface is a *two-dimensional* system). In this section we shall explore the ways in which fluctuations modify the mean-field phase diagrams. This will lead us to conjecture, at least qualitatively, what the exact interfacial phase diagrams and interfacial critical behavior for the model [Eq. (1)] should be.

The principle considerations which guide this extrapolation from mean-field results are the following.

(a) Exact results at $T=0$ and $T=T_c$. Section II C discussed $T=0$. As $T\to T_c^-$, the interfacial free energy vanishes as[38]

$$f_i(T,\hat{m})\sim A(T_c-T)^{(d-1)\nu}+\cdots , \tag{8}$$

where ν is the bulk correlation-length exponent ($\nu\simeq 0.63$ in $d=3$) and the ellipsis includes higher-order terms. The leading term is independent of $\hat{m}$, so both the Wulff plot and the ECS are spherical in this limit.

(b) Faceting and roughening of symmetry interfaces. Facets on the ECS come from cusps in the Wulff plot $f_i(\hat{m})$, which in turn are related to the existence of a nonzero free energy per unit length necessary to create a step or ledge on the corresponding facet.[3,39] Conversely, only steps on smooth, planar facets can have nonzero free energy per unit length.[40] Step free energies for $d=3$ (bulk) are positive at low temperature but vanish at a roughening temperature[14] $T_R(\hat{m})<T_c$, where the corresponding facet, therefore, disappears. For the NN model[14] ($R=0$), $T_R(100)\approx T_c/2$. The transition at T_R is second order and critical behavior is of the Kosterlitz-Thouless type.[12,14,41]

(c) The $d=2$ ANNNI model and its analogs. The ANNNI model[22,23] has a mean-field phase diagram which is very similar to Fig. 3. The ANNNI-model commensurate phases are analogous to the facets. (The competition between NN and axial NNN interactions in the ANNNI model is the analog of the competition between imposed tilt $\hat{m}$ and microscopic interface-energy considerations.) In the ANNNI-model context it is known that for $d=2$ the dense commensurate phases of mean-field theory are destroyed by fluctuations, leaving only two ordered phases (ferromagnetic and $\uparrow\uparrow\downarrow\downarrow$) separated by an incommensurate region. The expected analog for the crystal-shape problem is the destruction of the fully faceted polyhedra of the mean-field theory, leaving only $T=0$ facets separated by smoothly curved regions. Analogous behavior takes place in other $d=2$ models showing commensurate-incommensurate transitions.[42]

(d) Relevant excitations at second-order phase transitions. An understanding of the "relevant" excitations at second-order phase transitions allows plausible identification of universality classes. Thus it is known that because $T_R<T_c$, pure SOS-type interface excitations suffice to model the thermal-roughening transition.[12,14] We argue in a similar spirit that the (second-order) phase transitions associated with edges between faceted and curved parts of the interface are dominated by excitations of the step or ledge system introduced by Burton, Cabrera, and Frank.[9] The statistical mechanics of these excitations were first studied by Gruber and Mullins.[10] The analogous excitations in the commensurate-incommensurate problem are domain-wall excitations, as studied by Pokrovsky and Talapov[17] (stripe domains) and others.[11,18–21] The key common property of these systems is the absence of dislocation excitations, guaranteed in our model by the imposed lattice structure.[43–45] Most recently, SOS models incorporating both roughening and domain-wall excitations have been used by Jayaprakash, Saam, and Teitel[13] to study facet formation and facet shape near T_R. This beautiful work exploits the connection between the body-centered SOS (BCSOS) model[12] and the six-vertex models.[24,46]

(e) First-order stability. It is well known that first-order phase boundaries are relatively stable to fluctuation effects. It is, therefore, plausible to assume that first-order phase-diagram features are not qualitatively modified in going beyond mean-field theory.

A. $R=0$

Conjectured $(T,\hat{m})$ and $(T,\hat{h})$ phase diagrams for $R=0$ are shown in Figs. 6 and 7. Because only the $T=0$ facets remain [points (a)–(c)], the only cusps in the Wulff plot are at $\hat{m}=\{100\}$. These cusps disappear at a $\{100\}$ roughening temperature T_R [point (b)], above which the Wulff plot is entirely analytic [Figs. 6(a) and 7(a)]. This scenario leads to the evolution of crystal shape shown in Fig. 1 and represented in the phase diagrams of Figs. 6(b) and 7(b). Comparing Figs. 3 and 6(b), we see that T_R is now distinct from T_c, and the infinity of faceted (commensurate) phases present in mean-field theory has been suppressed by fluctuations.

The phase transitions in Figs. 6(b) and 7(b) are all second order. The thermal-roughening transition at $\hat{m}=(100)$ ($\theta=\phi=0$) is of the Kosterlitz-Thouless type [points (b) and (d)]. For fixed $T<T_R$, the phase boundary between the $\{100\}$ facets and the "rough" or curved regions corresponds to a $d=2$ commensurate-incommensurate transition [point d)]. The simple lattice structure of our model does not permit dislocations, so (in contrast, for example, to the $d=2$ ANNNI model[22]) the transition is expected to be in the Gruber-

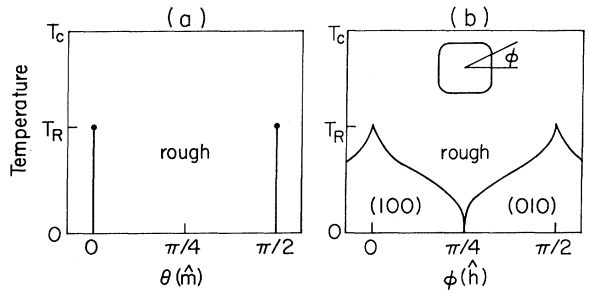

FIG. 6. (a) (T,θ) and (b) (T,ϕ) interfacial phase diagrams for $R=0$. θ and ϕ are angular variables which measure interfacial orientation ($\hat{m}$) and crystal shape ($\hat{h}$), respectively, in an equatorial section of the full three-dimensional phase diagram. The (T,θ) phase diagram (a) shows the locus of cusps in the Wulff plot along the symmetry directions for $T<T_R$. The (T,ϕ) phase diagram (b) plots the angular outline of the faceted areas of the crystal shape; it derives from the mean-field phase diagram (Fig. 3) after correction for fluctuation effects.

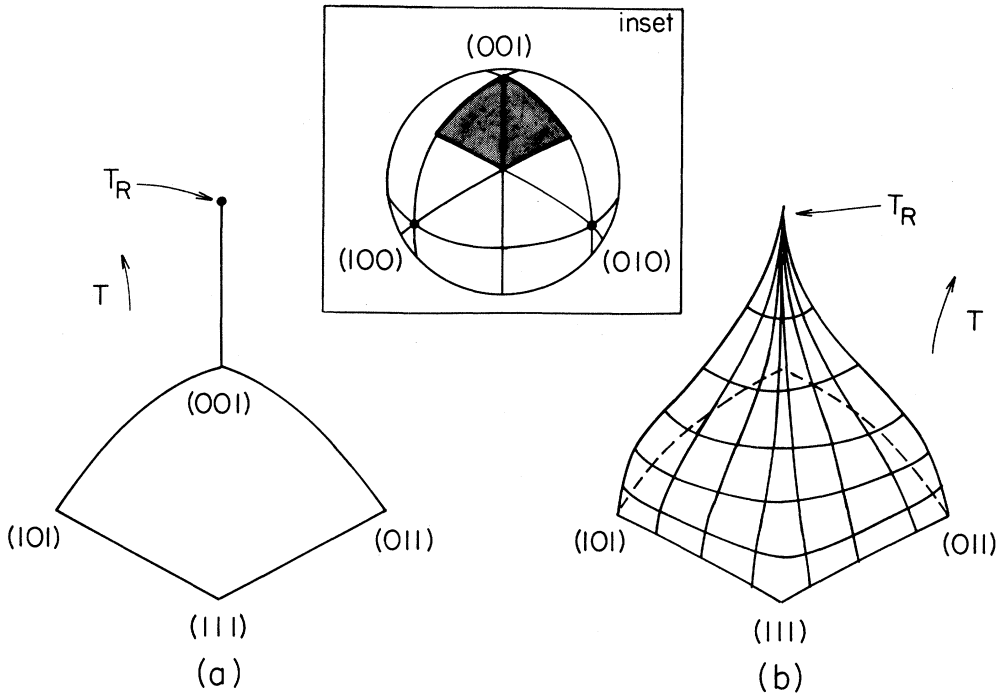

FIG. 7. (a) $(T,\hat{m})$ and (b) $(T,\hat{h})$ interfacial phase diagrams for $R=0$. The shaded portion in the inset indicates the range of orientations $\hat{m}$ and $\hat{h}$ included in the plots. The $(T,\hat{m})$ phase diagram is a set of spikes of length T_R in the $\{100\}$ directions. The $(T,\hat{h})$ phase diagram is a curved surface, cusped in the symmetry directions ($\{100\}$), with $T=$const cross sections which become circular as $T\to T_c^-$.

Mullins–Pokrovsky-Talapov universality class.[10,17,47] Critical behavior corresponds to free fermions[17,21,35,48] in $d=1$ and is well known. The free energy connects with the crystal shape[27] $r(T,\hat{h})$, and its singularity describes the behavior of the ECS near the facet edge[49] (Fig. 8),

$$y\sim x^{\theta} \text{ with } \theta=\tfrac{3}{2} , \tag{9}$$

which is quite different from the continuum mean-field result[27] $\theta_{\rm MF}=2$. Finally, near the special point $T=T_R,\phi=0$, both types of excitations are present [point (d)] and the phase boundary behaves as[13,50]

$$\phi_c\sim\exp[-A/(T_R-T)^{1/2}] , \tag{10}$$

which produces the pointed $(T,\hat{h})$ phase boundaries. Crossover behavior has recently been worked out in detail for certain SOS models,[13] and includes a universal jump in interfacial curvature as $T\to T_R^+$.

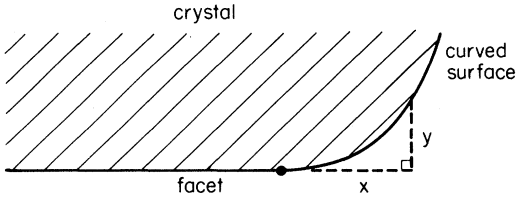

FIG. 8. Schematic cross section through a smooth edge in the ECS, where a facet meets a curved surface. Near the edge the shape of the curved surface is described by $y\sim x^{\theta}$. The exponent θ is a critical index.

B. $R\neq 0$

Modification of the mean-field phase diagram for $R\neq 0$ proceeds similarly, again using points (a)–(e) above. For $R>0$, additional facets are present at $T=0$ (Sec. II C). These principal symmetry facets persist for $T>0$, while the remaining mean-field faceting is suppressed by fluctuations. Each symmetry facet roughens out at its own T_R. The (T,θ) phase diagram [Fig. 9(a)] picks up the Wulff-plot cusps associated with the $\{100\}$ and $\{110\}$ (but not $\{111\}$) facets. (T,ϕ) and $(T,\hat{h})$ phase diagrams are sketched in Figs. 9(b) and 10(b). Phase transitions are all second order and of the same types as for $R=0$. The pointed shape of the phase boundaries near roughening

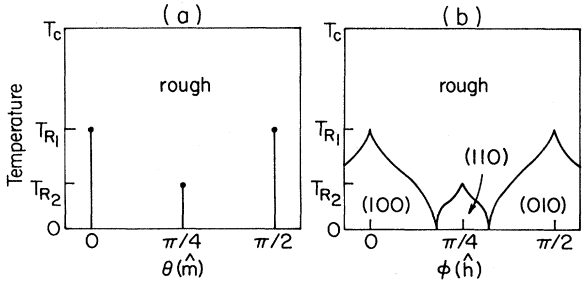

FIG. 9. (a) (T,θ) and (b) (T,ϕ) interfacial phase diagrams for $R=0.1$. Variables are same as in Fig. 6. The (T,ϕ) phase diagram (b) is a fluctuation-corrected version of Fig. 4. The additional (110) facet is present at low temperature and disappears at its own characteristic roughening temperature T_{R_2}. $\{111\}$ facets do not show up in this equatorial cut.

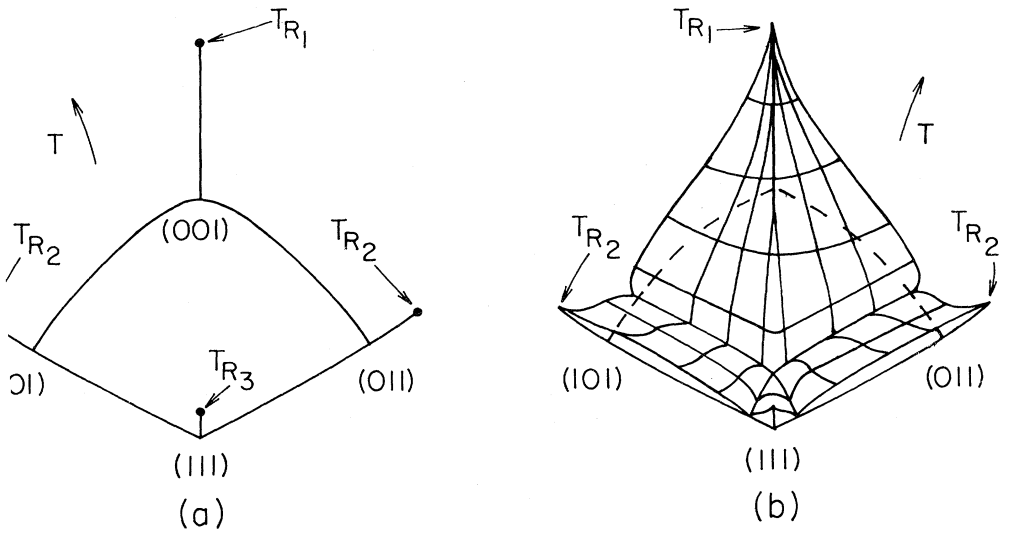

FIG. 10. (a) $(T,\hat{m})$ and (b) $(T,\hat{h})$ interfacial phase diagrams for $R=0.1$. Variables are same as Fig. 7. Additional {110} and {111} facets are present at sufficiently low temperatures. Figure 9 is a cross section of Fig. 10. The observed phase diagram of hcp ^{4}He appears to be of this generic type.

follows from Eq. (10). The corresponding ECS (Fig. 1) loses its sharp $T=0$ edges for all $T>0$. Symmetry facets roughen out, each at its own characteristic T_R. Above the last roughening temperature (presumably $\hat{m}=\{100\}$ for small R), the ECS is smoothly rounded and approaches sphericity as $T\to T_c^-$. It seems clear that adding additional further-neighbor attractive interactions should simply produce new $T=0$ facets, each disappearing at its own T_R, as seen in recent experiments[6] on hcp ^{4}He.

The procedure is similar for $R<0$ only here because of the sharp (first-order) edges which occur at low temperatures in the mean-field treatment (Sec. III and Fig. 5), point (e) takes effect. Thus we retain in Figs. 11 and 12 the low-temperature features of mean-field theory qualitatively intact. The crystal shape (Fig. 1) remains cubical at low temperature ($T<T_0$). At T_0, a curved region using {111} and nearby directions first appears at the cube corners, surrounded by sharp (first-order) edges. This rounded region grows as T increases and finally intersects the equatorial plane at $T=T_3$. At higher temperatures the edges become smooth, starting (if mean-field theory is a reliable guide) near the {111} direction and progressing towards the equatorial plane. For $T_t<T<T_R$ all edges are smooth, just as for $R\geq 0$. A line of multicritical points separates first- and second-order behavior [T_t in Fig. 11(b) and the boundary of the shaded region in Fig. 12(b)]. Our calculation is the first to find first-order behavior in the context of equilibrium crystal shapes. Figures 11(a) and 12(a) exhibit the corresponding $(T,\hat{m})$ phase diagram. Note that the region below the curved line in Fig. 11(a) [and underneath the curved surface in Fig. 12(a)] is "forbidden" in the sense that corresponding interfacial orientations are not attainable at equilibrium, as discussed at the close of Sec. I.

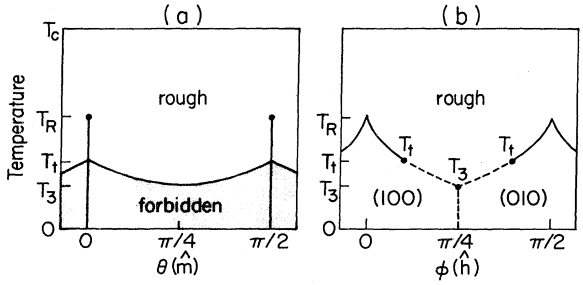

FIG. 11. (a) (T,θ) and (b) (T,ϕ) interfacial phase diagrams for $R=-0.1$. {100} facets are stabilized up to a nonzero temperature T_0. Curved surfaces first appear at cube corners and then reach the equatorial plane at T_3. The transition at the equator remains first order until a higher temperature T_t. First-order phase boundaries are shown dashed. Note appearance of the forbidden region in (a). The mean-field phase diagram corresponding to (b) is Fig. 5.

ACKNOWLEDGMENTS

We acknowledge, with thanks, helpful conversations with D. B. Abrahams, M. P. M. den Nijs, H. J. Hilhorst, D. Huse, C. Jayaprakash, B. Nienhuis, W. F. Saam, and J. Weeks. This work was supported in part by the National Science Foundation under Grants Nos. DMR-80-20250 and DMR-81-17182.

APPENDIX

Mean-field theory involves the global minimization of the variational functional,[51]

$$\mathcal{F}(\{\mathcal{M}_i\})=-J_1\sum_{\substack{\langle ij\rangle\\ \text{NN}}}\mathcal{M}_i\mathcal{M}_j-J_2\sum_{\substack{\langle ij\rangle\\ \text{NNN}}}\mathcal{M}_i\mathcal{M}_j$$
$$+k_BT\sum_i\int_0^{\mathcal{M}_i}dy\,\tanh^{-1}y\ . \qquad \text{(A1)}$$

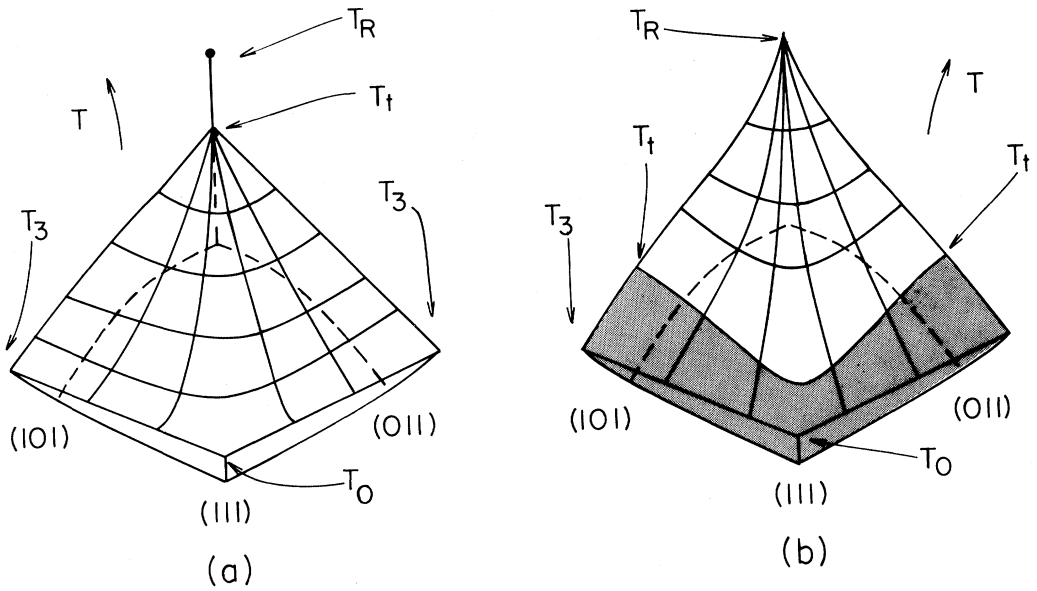

FIG. 12. (a) $(T,\hat{m})$ and (b) $(T,\hat{h})$ interfacial phase diagrams for $R=-0.1$. In the $(T,\hat{m})$ phase diagram the forbidden region is underneath curved surface. In (b) first-order boundaries (shaded) join a second-order region at a line of multicritical points. Figure 11 corresponds to the equatorial section of this plot.

In the bulk each site is equivalent. By setting $\mathcal{M}=\mathcal{M}_b$ for all i, Eq. (A1) becomes

$$\mathcal{F}_b(\mathcal{M}_b)=N\left[(-6J_1-12J_2)\mathcal{M}_b^2 + k_BT\int_0^{\mathcal{M}_b} dy\,\tanh^{-1}y\right] . \tag{A2}$$

Here, N is the number of sites. At the global minimum of Eq. (A2) the bulk magnetization at site i is $\mathcal{M}_b^{\min}$ and the bulk free-energy density is $f_b=\mathcal{F}_b(\mathcal{M}_b^{\min})/N$. $\mathcal{M}_b^{\min}$ is easily found by iterating the bulk mean-field equation, which is the rearrangement of the equation $\partial\mathcal{F}_b/\partial\mathcal{M}_b=0$,

$$\mathcal{M}_b=\tanh[(6J_1+12J_2)\mathcal{M}_b/(k_BT)] . \tag{A3}$$

In the presence of an interface, the magnetizations vary from site to site. Assuming the tilt is only in one direction, we may let

$$\mathcal{M}_i=\mathcal{M}(i_x,i_y,i_z)=\mathcal{M}(i_x,i_y,i_z+1)\equiv\mathcal{M}(i_x,i_y) .$$

We chose the angle θ such that $\tan\theta=p/q$, where p and q are relatively prime and $p<q$. Let $1\le i_x\le n_x$ and $1\le i_y\le n_y$ define the sample size, where $n_y>n_x$ and $n_x=l_xq$ (see Fig. 13). The boundaries are taken to be antiperiodic in the $\hat{y}$ direction,

$$\begin{aligned}&\mathcal{M}(i_x,0)=-\mathcal{M}(i_x,n_y),\quad 1\le i_x\le n_x\\ &\mathcal{M}(i_x,n_y+1)=-\mathcal{M}(i_x,1),\quad 1\le i_x\le n_x .\end{aligned} \tag{A4}$$

A tilt is forced by using displaced periodic and antiperiodic boundary conditions in the $\hat{x}$ direction,

$$\begin{aligned}&\mathcal{M}(0,i_y)=\mathcal{M}(n_x,i_y+l_xp) ,\\ &\mathcal{M}(n_x+1,i_y+l_xp)=\mathcal{M}(1,i_y),\quad 1\le i_y\le n_y-l_xp\\ &\mathcal{M}(0,i_y)=-\mathcal{M}(n_x,i_y-n_y+l_xq) ,\\ &\mathcal{M}(n_x+1,i_y-n_y+l_xq)=-\mathcal{M}(1,i_y),\ n_y-l_xp+1\le i_y\le n_y .\end{aligned} \tag{A5}$$

Stationary solutions of Eq. (A1) may be found by beginning with a particular set $\{\mathcal{M}_i\}$ and iterating the stationarity equation which follows from $\partial\mathcal{F}/\partial\mathcal{M}_i=0$, namely,

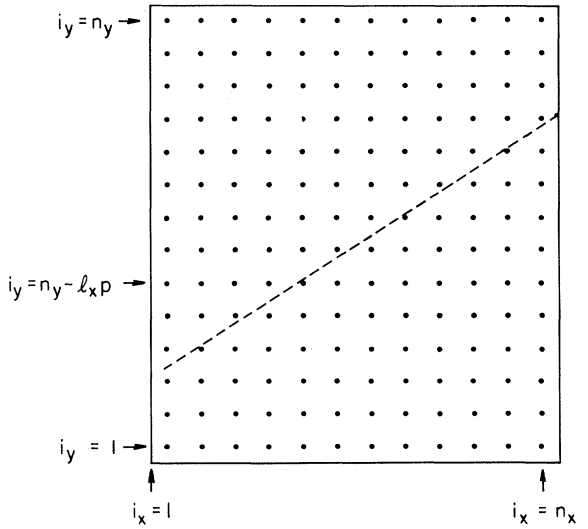

FIG. 13. Geometry used to find interfacial free energy f_i. Dotted line indicates the orientation of the interface. Variables of the Appendix corresponding to this figure are $q=3$, $p=2$, $l_x=4$, $n_x=12$, and $n_y=14$.

$$\mathcal{M}_i = \tanh\left[\left[J_1 \sum_{\substack{j \text{ NN} \\ \text{to } i}} \mathcal{M}_j + J_2 \sum_{\substack{j \text{ NNN} \\ \text{to } i}} \mathcal{M}_j\right] \Big/ k_B T\right], \quad \text{(A6)}$$

with the boundary conditions (A4) and (A5). Of the solutions which satisfy Eq. (A6), the one which minimizes Eq. (A1), $(\mathcal{F})_{\min}$, is found. Then f_i may be found as follows:

$$f_i(l_x,\theta,T,R) = \lim_{n_y\to\infty} \frac{(\mathcal{F})_{\min} - n_x n_y f_b}{n_x/\cos\theta},$$

$$f_i(\theta,T,R) = \lim_{n_x\to\infty} f_i(l_x,\theta,T,R).$$

For a given T,R,θ, a large number of solutions to Eq. (A6) may be found. From a practical point of view it is necessary to investigate the periodicity of the mean-field solution [the global minimum of Eq. (A1)] and its relationship to the minimum periodicity possible (which is determined by p and q). We found that, when the value of (T,θ) corresponds to a "forbidden" region [see Fig. 11(a)], $f_i(l_x,\theta,T,R)$ was minimized for $l_x=\infty$, while, for the single-phase region, $f_i(l_x,\theta,T,R)$ is independent of l_x. For example, when $\theta=\pi/4$ the mean-field free energies $f_i(N)$ may be calculated, corresponding (only approximately for $T>0$) to interfaces which alternate between N steps in the x direction and N steps in the $\hat{y}$ direction. We find that, as a function of N, $f_i(N)$ is minimized for either $N=1$ or ∞. Of course, in the latter case $f_i(\infty)$ is simply $f_i(\theta=0)/\sqrt{2}$, that of two perpendicular, flat interfaces.

*Present address: Department of Physics, 174 W. 18th Avenue, Ohio State University, Columbus, OH 43210.

[1]C. Herring, Phys. Rev. 82, 87 (1951).

[2]C. Herring, in *Structure and Properties of Solid Surfaces,* edited by R. Gomer and C. S. Smith (University of Chicago Press, Chicago, 1953), pp. 5–72.

[3]C. Rottman and M. Wortis, Phys. Rep. (to be published). This review contains many literature citations and a general exposition of the "phase-diagram" approach to equilibrium crystal shapes.

[4]Additional possibilities (see Refs. 1 and 2) include two or more rounded regions joined at edges, "ruled" surfaces, etc. These do not seem to occur for the model we shall consider herein.

[5]J. C. Heyraud and J. J. Metois, Acta Metall. 28, 1789 (1980); J. Cryst. Growth 50, 571 (1980); 57, 487 (1982); Surf. Sci. 128, 334 (1983); J. J. Metois, G. Le Lay, Surf. Sci. (to be published).

[6]K. O. Keshishev, A. Ya. Parshin, and A. I. Shal'nikov, in *Soviet Scientific Reviews, Section A: Physics Reviews,* edited by I. M. Khalatnikov (Harwood Academic, Chur, 1982), Vol. 4, pp. 155–218, which contains earlier references on ^{4}He crystal shapes.

[7]C. Rottman and M. Wortis, Phys. Rev. B 24, 6274 (1981); J. E. Avron, H. van Beijeren, L. S. Schulman, and R. K. P. Zia, J. Phys. A 15, L81 (1982); R. K. P. Zia and J. E. Avron, Phys. Rev. B 25, 2042 (1982).

[8]A survey of $T=0$ work on short-ranged potentials may be found in S. Tochev, in *Crystal Growth: An Introduction,* edited by P. Hartman (North-Holland, Amsterdam, 1973), pp. 328–341; P. Bennema, *ibid.*, pp. 342–357. It has been argued [D. S. Fisher and J. D. Weeks, Phys. Rev. Lett. 50, 1077 (1983); E. Frankin, Phys. Rev. B (to be published)] that quantum crystals are completely faceted at $T=0$ as well.

[9]W. K. Burton, N. Cabrera, and F. C. Frank, Philos. Trans. R. Soc. London Ser. A 243, 299 (1951). See also, J. Frenkel, J. Phys. (Paris) 9, 392 (1945).

[10]E. E. Gruber and W. W. Mullins, J. Phys. Chem. Solids 28, 875 (1967).

[11]H. W. J. Blöte and H. J. Hilhorst, J. Phys. A 15, L631 (1982).

[12]H. van Beijeren, Phys. Rev. Lett. 38, 993 (1977).

[13]C. Jayaprakash, W. F. Saam, and S. Teitel, Phys. Rev. Lett. 50, 2017 (1983); W. F. Saam, C. Jayaprakash, and S. Teitel, AIP Proceedings of the 1983 Sanibel Symposium on Quantum Fluids and Solids (to be published).

[14]For a recent review of roughening, see J. D. Weeks and G. H. Gilmer, in *Advances in Chemical Physics,* edited by I. Prigogine and S. A. Rice (Wiley, New York, 1979), pp. 190–197.

[15]R. Lacmann, in *Springer Tracts in Modern Physics,* edited by G. Hohler (Springer, New York, 1968), Vol. 44, pp. 1–82; J. Cryst. Growth 3, 523 (1968).

[16]J. W. Cahn and J. E. Hilliard, J. Chem. Phys. 28, 258 (1958); H. Müller-Krumbhaar, Phys. Rev. B 10, 1308 (1974).

[17]V. L. Pokrovsky and A. L. Talapov, Phys. Rev. Lett. 42, 65 (1979); Zh. Eksp. Teor. Fiz. 78, 269 (1980) [Sov. Phys.—JETP 51, 134 (1980)].

[18]S. Ostlund, Phys. Rev. B 24, 398 (1981).

[19]H. J. Schultz, Phys. Rev. Lett. 46, 1685 (1981).

[20]F. D. M. Haldane and J. Villain, J. Phys. (Paris) 42, 1673 (1981).

[21]M. P. M. den Nijs, in Phase Transitions and Critical Phenomena, edited by C. Domb, M. S. Green, and J. L. Lebowitz (unpublished).

[22]For a review of work on the ANNNI model, see P. Bak, Rep. Prog. Phys. 45, 587 (1982).

[23]P. Bak and J. von Boehm, Phys. Rev. B 21, 5297 (1980); J. Villain and P. Bak, J. Phys. (Paris) 42, 657 (1981).

[24]E. H. Lieb and F. Y. Wu, in *Phase Transitions and Critical Phenomena,* edited by C. Domb and M. S. Green (Academic, London, 1972), Vol. 1, pp. 331–490.

[25]G. Wulff, Z. Kristallogr. Mineral. 34, 449 (1901).

[26]See Ref. 9, Appendix D.

[27]A. F. Andreev, Zh. Eksp. Teor. Fiz. 80, 2042 (1981) [Sov. Phys.—JETP 53, 1063 (1982)].

[28]M. Flytzani-Stephanopoulas and L. D. Schmidt, Prog. Surf. Sci. 9, 83 (1979); G. A. Somorjai, *Chemistry in Two Dimensions* (Cornell University Press, Ithaca, 1981), pp. 162–168.

[29]N. Cabrera, *Symposium on Properties of Surfaces* (American Society for Testing and Materials, Philadelphia, 1963), pp. 24–31.

[30]K. Huang, *Statistical Mechanics* (Wiley, New York, 1963), pp. 332–334.

[31]P. G. Watson, in *Phase Transitions and Critical Phenomena,* Ref. 24, Vol. 2, pp. 101–159.

[32]This is one of several equivalent definitions. For alternatives, see citations in Refs. 3 and 31.

[33]Exploration of the {111} direction is necessary to understand the $R<0$ phase diagrams. See below.

[34]A particularly simple derivation of Eq. (5) with $R=0$ may be found by W. W. Mullins, in *Metal Surfaces: Structures, Energetics, and Kinetics* (American Society for Metals, Metals

Park, Ohio, 1963), pp. 17–66.

[35]J. B. Kogut, D. K. Sinclair, R. B. Pearson, J. L. Richardson, and J. Shigemitsu, Phys. Rev. D 23, 2945 (1981); J. B. Kogut and D. K. Sinclair, *ibid.* 24, 1610 (1981).

[36]We do not, of course, claim to have established these as rigorous properties of mean-field theory. Although such a demonstration would be interesting, its importance is mitigated by the fact that these features are modified by fluctuations. See Sec. IV.

[37]Notice in this connection the convenience of working with the $(T,\hat{h})$ phase diagram rather than the $(T,\hat{m})$ phase diagram, which would have been quite impossible to explore numerically.

[38]B. Widom, J. Chem. Phys. 43, 3892 (1965).

[39]D. TerHaar, *Collected Papers of L. D. Landau* (Gordon and Breach, New York, 1965), pp. 540–545.

[40]H. J. Leamy and G. H. Gilmer, J. Cryst. Growth 24-25, 499 (1974).

[41]J. V. Jose, L. P. Kadanoff, S. Kirkpatrick, and D. Nelson, Phys. Rev. B 16, 83 (1979).

[42]The central feature here is the destruction of the high-order commensurate phases by fluctuations in $d=2$. This destruction—of which the ANNNI model is a well-documented example—does not depend on the presence or absence of dislocations. See, however, point (d) below and Ref. 44.

[43]The presence of dislocations would imply that the nominal height difference between two points on the interface might depend on the path along the interface used to join them. For a perfect (bulk) lattice this is geometrically impossible.

[44]When dislocations are allowed (as, for example, for the ANNNI model, Ref. 22) they change the universality class of the phase transition. See Ref. 21.

[45]Surfaces penetrated by screw dislocations can and do exhibit interfacial dislocation structure. Such dislocations are pinned or "frozen in" by the bulk lattice structure and not, therefore, equivalent to the free dislocations which play a role in $d=2$ melting. Small metal crystals can apparently be grown free of screw dislocations (Ref. 5). The theory presented here should apply to such crystals but would require modification if applied to crystals with a bulk density of dislocations.

[46]B. Sutherland, C. N. Yang, and C. P. Yang, Phys. Rev. Lett. 19, 588 (1967).

[47]Gruber and Mullins (Ref. 10) did not, in fact, work through the critical behavior predicted by their model of interacting steps. Indeed, they did not think of such behavior in terms of phase transition. Nevertheless, the free fermions which give $\theta=\frac{3}{2}$ [Eq. (9)] are clearly visible in their appendix.

[48]P. G. deGennes, J. Chem. Phys. 48, 2257 (1968); J. Villain, in *Ordering in Strongly Fluctuating Condensed Matter Systems,* edited by T. Riste (Plenum, New York, 1980), pp. 221–260.

[49]The usual form of this result in the commensurate-incommensurate context is that the density of domain walls (analogous to θ) vanishes with the square root of the chemical potential difference [analogous to $(\phi-\phi_c)$]. This is just the derivative of Eq. (9).

[50]M. P. M. den Nijs (private communication).

[51]This form of the variational functional $\mathcal{F}$ may be obtained by using the methods described in H. Falk, Am. J. Phys. 38, 858 (1970).